FRACTURE PROCESS ZONE IN CONCRETE TENSION SPECIMENS BY X-RAY AND AE TECHNIQUES

K. Otsuka, H. Date, and T. Kurita
Department of Civil Engineering, Tohoku-Gakuin University, Tagajo
Japan

Abstract
Experiments were carried out with an x-ray using contrast medium and three-dimensional acoustic emission (AE) techniques to investigate the behavior of the fracture process zone in concrete. The results show that, as the loading increases, a fracture process zone consisting of numerous micro cracks or AE events develops ahead of the tip of the notch cut in the concrete compact tension specimen. The maximum width of the microcrack zone is strongly related to the maximum aggregate size of the concrete. The energy of each individual AE event was calculated and plotted on the three- dimensional map. The results obtained by the two methods were compared and related to provide a clear view of the fracture process zone of concrete.
Key words: Fracture process zone, X-ray, AE (acoustic emission),

1 Introduction

A general consensus exists in relating the fracture behavior of concrete to a fracture process zone that develops around and ahead of the main crack tip. However, a direct quantitative relationship between the process-zone

characteristics and the measured toughness cannot yet be established. It has recently been thought that an important task in the future development of the fracture mechanics of concrete is to standardize the testing procedure. The length and the width of the fracture process zone are crucial in selecting the geometry and dimensions of the standard test specimen. Many authors have already experimentally investigated the fracture process zone. However, there are significant discrepancies in these results. Such discrepancies have probably resulted from differences in the observation techniques employed. There are many different observation techniques, including optical microscopy, electron microscopy, acoustic emission techniques, and laser speckle techniques.

It is very important to observe the internal fractures in concrete. The x-ray technique using contrast medium can directly inspect the internal fractures in concrete. AE is not a direct observation technique, but it also allows for the inspection of internal fractures in concrete. This paper reports an investigation of the fracture process zone using two methods: the direct observation X-ray technique and the indirect observation AE technique. Both allow for the inspection of internal fractures in concrete. The results obtained from the two methods are compared and related to provide a clear view of the fracture process zone of concrete.

2 Test procedure

2.1 Specimens

Concrete containing high-early-strength Portland cement was used. The fine aggregate was a river product, and the coarse aggregate was a crushed stone product. The maximum size of the coarse aggregate was 10 or 20 mm. All specimens were made from concrete with a specified cylinder strength of f'c=20 Mpa. Relatively low-strength concrete was used to make clear the effects of maximum aggregate size on the fracture befavior of concrete. A p-wave velocity of 3600 m/s was decided upon for the
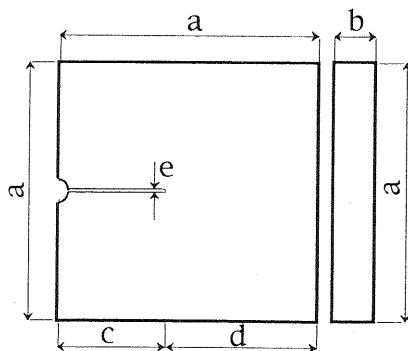
Table 1. Dimensions of specimens

	S type	M type	L type
a	175	350	525
b	80	80	80
c	92	185	276
d	83	165	249
e	5	5	5

Fig. 1. Configuration of specimen

concrete after a preparatory experiment.

Figure 1 shows the configuration of the specimens used in the test. Three different-sized specimens, S-type, M-type and L-type, were prepared to examine the effect of specimen size on the behavior of the fracture process zone.

Table 1 shows the dimensions of the specimens. In the x-ray investigation, all three types of specimens were used. In the AE investigation, S-type and M-type specimens were used.

2.2 X-ray inspection technique

Figure 2 shows an example of the specimens used in the x-ray investigation. The x-ray inspection consisted of pumping a contrast medium into the injection holes in the concrete specimen before loading, and performing radiography at several stages during loading.
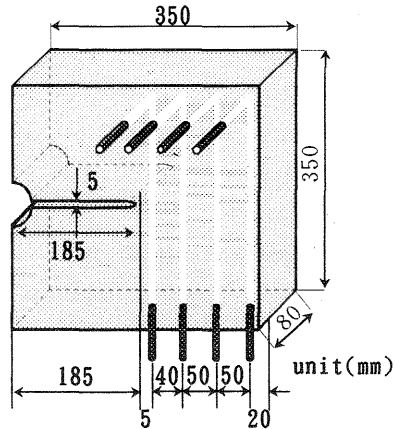

Fig. 2. Contrast medium injection holes

2.3 AE inspection technique

Locations of the points where AE (acourstic emission) events occurred were measured by a three-dimensional AE system (Fig. 3). The system consisted of sensors, preamplifiers , a local processor, a digital data recorder, and an AE analyzer. Four channels were employed. Figure 4 shows the location of the four sensors on the specimen. All sensors were of the resonant frequency 140 kHz. A 70-dB gain was used for amplification .
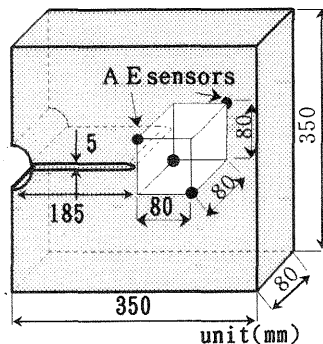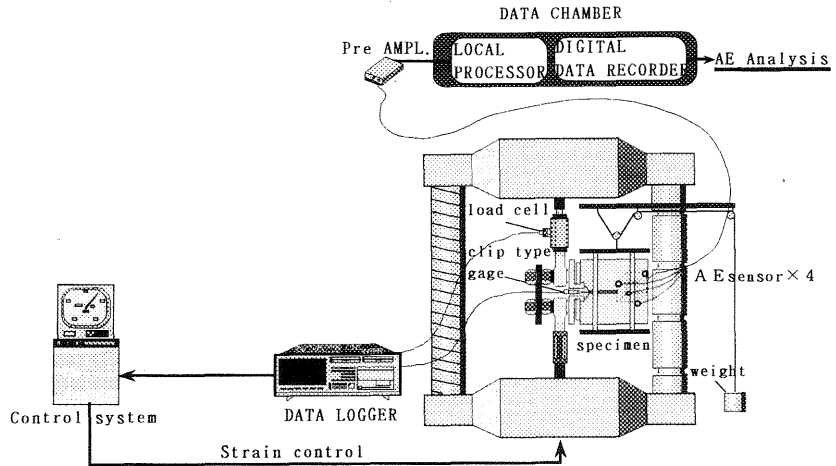

Fig. 3. Location of sensors

5

Fig. 4. AE measurement system

2.4 Loading equipment

A universal testing machine was used for loading. The specimen was loaded under strain control at a rate of 0.005 mm of crack-opening displacement per minute. The specimen was loaded through two steel plates that were bonded to the specimen using an adhesive agent.

3 Test results

3.1 X-ray inspection

3.1.1 Behavior of the fracture process zone

Figure 5 shows an example of a load to crack opening displacement(COD) relationship measured from a M-type specimen. The maximum aggregate size of the concrete was 20 mm. X-ray inspections were made at points P1 (70% of peak load), P2 (peak load), P3 (70% of peak load) , and P4 (30% of peak load) on the curve.
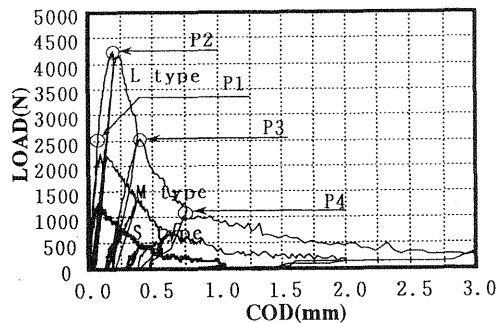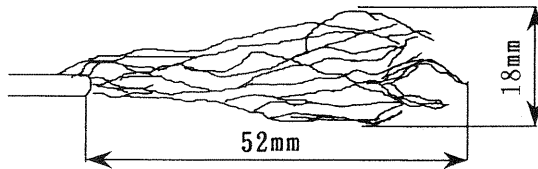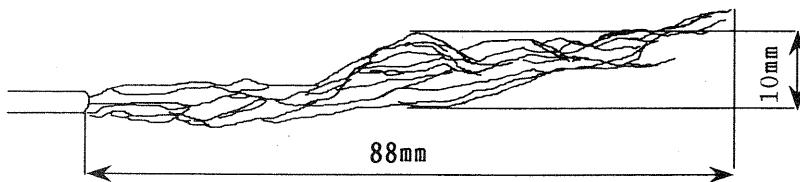

Fig. 5. Load-displacement curves of specimen

3.1.2 Influence of maximum aggregate size on the fracture process zone

Figure 7 shows two cracks-zone shapes traced from the x-ray films of two different specimens obtained at peak load. Each was an M-type specimen made from concrete with different maximum aggregate sizes of10 mm, Fig. 7(a), and 20 mm, Fig. 7(b). As can be seen in these figures, the widths of the cracks zone differ according to the maximum aggregate size, increasing with an increase in the maximum aggregate size. The ratio of these crack-zone widths is 1.0 : 1.8 . In contrast, the length of the crack zone decreases with an increase in the maximum aggregate size. The ratio of these crack-zone lengths is 1.0 : 0.6.
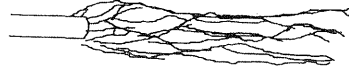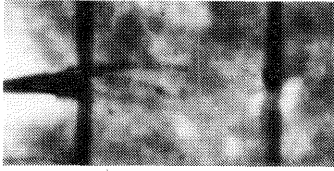
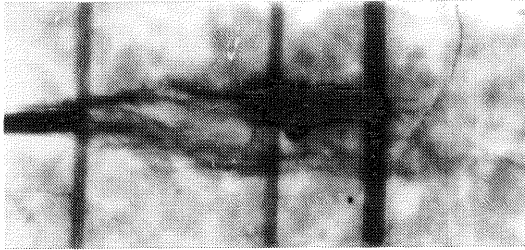(a) Maximum aggregate size: 20mm

(b) Maximum aggragete size: 10 mm

Fig. 7. Shapes of cracks zone obtained by x-ray technique
(M type specimn, at peak load)

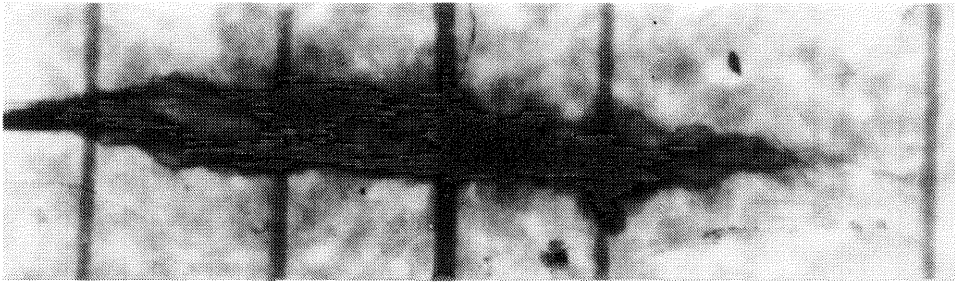3.1.3 Influence of specimen size on the fracture process zone

Figure 8 shows three shapes of crack zones traced from the x-ray films of three different specimens obtained at peak load. These specimens were S-type, Fig. 8(a), M-type, Fig. 8(b), and L-type, Fig. 8(c). They were made from concrete with a maximum aggregate size of 10 mm. As can be seen in these figures, the shapes of fine crack zones increase according to an increase in specimen size. The ratios of the length of the fine crack zone is 1 : 2.5 : 6.3 and of the width of the fine crack zone is 1 : 2.5 : 3.0 for S-type, M-type, and L-type specimens. The width of the fine crack zone of the S-type specimen was very small. The aggregate size of the concrete for these three specimens was 10 mm. It is tought that the size of the

(a) Cracks at the peak load

(b) Cracks at the 0.7 post-peak load

(c) Cracks at the 0.3 post-peak load

Fig. 6. Cracks zone obtained by x-ray technique with contrast medium.
(M type specimen, maximum aggregate size:10mm, at peak load)

Figure 6 shows an example of results obtained by x-ray inspection. On the x-ray films, microcracks forming at the tip of the notch were observed at about 0.8-peak load . Figure 6(a) shows a photograph printed from the x-ray film taken at the peak load and a figure traced directly from the film.

Figure 6(b) and 6(c) show photographs and traced figures of the 0.7 and 0.3 post-peak loads, respectively. Many fine cracks in a complex configuration near the tip of the notch were inspected and they gradually increased as the load stages progressed.

fracture process zones is strongly related to the maximum aggregate size. Therefore the widths of the fine crack zone should not be significantly different . The authors consider that the size of the S-type specimen was not sufficient to develop the fracture process zone of the concrete. It is thought that a proper specimen size may exist to develop a correct fracture process zone in concrete.
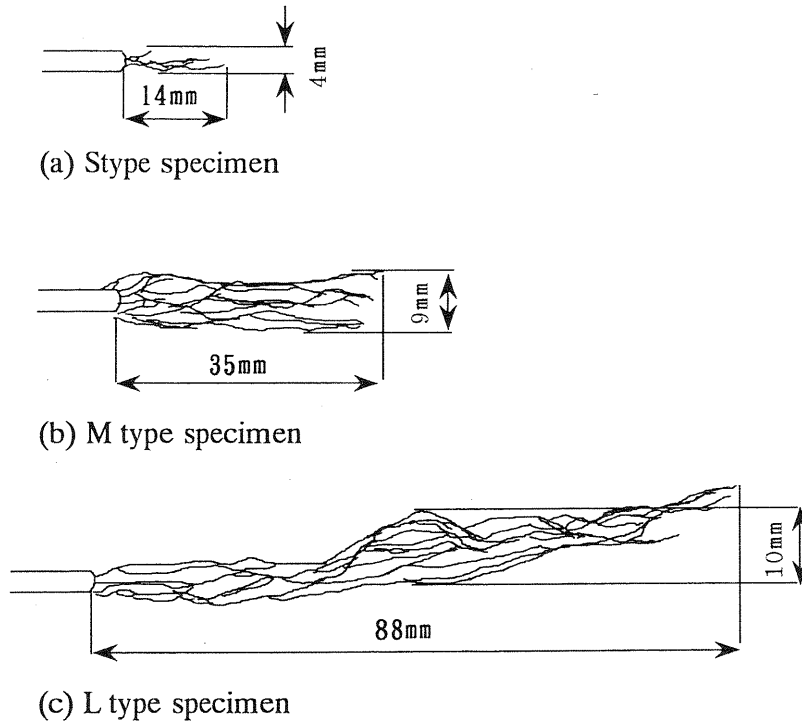
(a) Stype specimen

(b) M type specimen

(c) L type specimen

Fig.8. shapes of cracks zone obtained by x-ray technique
.(S, M and L types, maximum aggregate size: 10 mm, at peak load)

3.2 AE inspection

3.2.1 Behavior of the fracture process zone
Figure 9 shows an example of the load-to-crack opening displacement relationship measured from M-type specimens made from a concrete with a maximum aggregate size of 10 mm. AE inspection s were made at the numbered points on the curve. In this figure, the number of accumulated AE events is plotted. After the maximum load, the AE activity increased rapidly. Approximately 80 % of the total AE counts could be used to determine the three-dimensional location of the AE event.
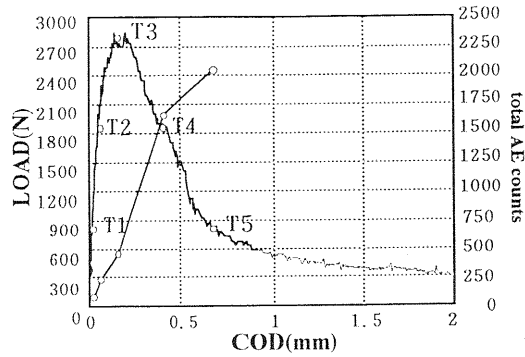
9

Fig. 9 Load -crack opening displacement curve and total AE counts curve

Figure 10 shows typical results obtained from an M-type specimen with a maximum aggregate size of 10 mm. The maps of the AE event source location at five stages of the loading are plotted in the figure. This figure shows the AE events that occurred between zero to 0.3 peak load (Fig. 10 (a)), 0.3 to 0.7 peak load (Fig. 10(b)), 0.7 to peak load (Fig. 10(c)), peak load to 0.7 post- peak load (Fig. 10(d)), and 0.7 post- peak load to 0.3 post-peak load (Fig. 10(e)). It is shown that the AE events occured at the

(a) T1(0-0.3 peak load)   (b) T2(0.3-0.7 peak load)   (c) T3(0.7-peak load)

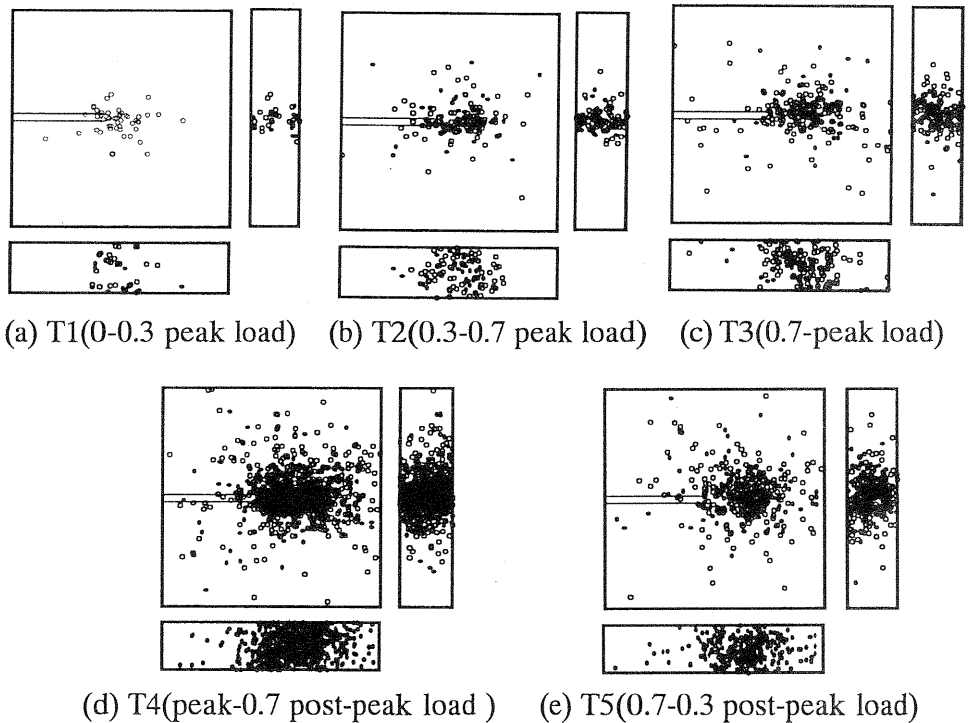(d) T4(peak-0.7 post-peak load)   (e) T5(0.7-0.3 post-peak load)
Fig. 10. Maps of all AE events source location.

tip of the notch even for the first period. The majority of AE events that registered in the period between the 0.7 pre-peak load and the 0.7 post-peak load showed a tendency to concentrate around the tip of the notch. After this period, the AE map showed a widely spread distribution . It can be said from maps of the two side plan in Fig. 10(c) that the distribution of AE events at the direction of thickness of specimen is nearly the same.

3.2.2 AE energy

The energy of individual events can be calculated from the square of the amplitude of the wave multiplied by the continuance time of the wave. Table 2 shows the caluculated energy of AE events. The wave occurring at an event source was measured by four sensors. The four values of calculated energies were not significantly different , and the largest value was adopted. All the AE events were divided into five stages of energy levels. The energies of AE events at each energy level and their percentage in relation to the total energy were calculated for the M-typespecimens (Table 2). The distribution of the AE event numbers at each energy stage are plotted in Fig. 8. Though 45 % of all AE events occurred at the stage below an energy of 100 volt$^2\mu$ s , the total energy of these events was only 0.5 % of the total energy of all events, indicating that the energy of each event was very small. The authors belive that these very small energy AE events are not directly related to the fracture process zone.

<div align="center">Table. 2. Calculated energy</div>

energy stages unit:(V$^2 \cdot \mu$ s)	event number		total energy		accumulation(%)
	number	%	number (V$^2 \cdot _{\mu s}$)	%	
total	2038	(100)	4.8834*10^6	(100)	
E1	919	(45.1)	2.2321*10^4	(0.5)	100.0
E2	558	(27.4)	2.1138*10^5	(4.3)	99.5
E3	373	(18.3)	1.2975*10^6	(26.6)	95.2
E4	73	(3.6)	9.0577*10^5	(18.5)	68.6
E5	115	(5.6)	2.4464*10^6	(50.1)	50.1

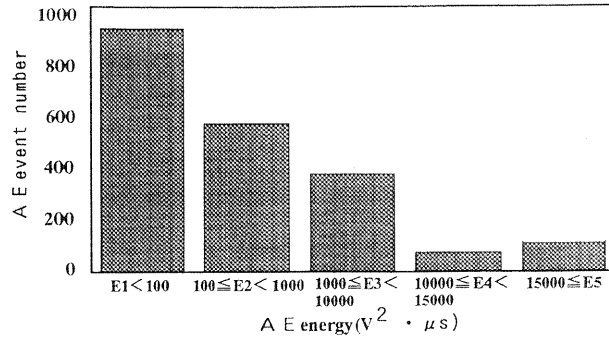E1;E1< 100   E2;100 ≦ E2 < 1000   E3;1000 ≦ E3 < 10000   E4;10000 ≦ E4 < 15000   E5;15000 ≦ E5
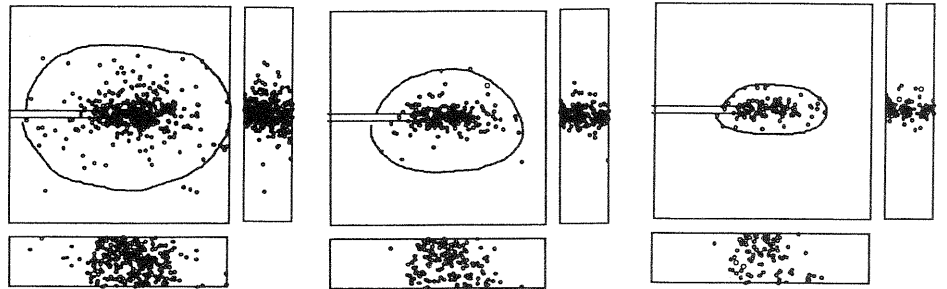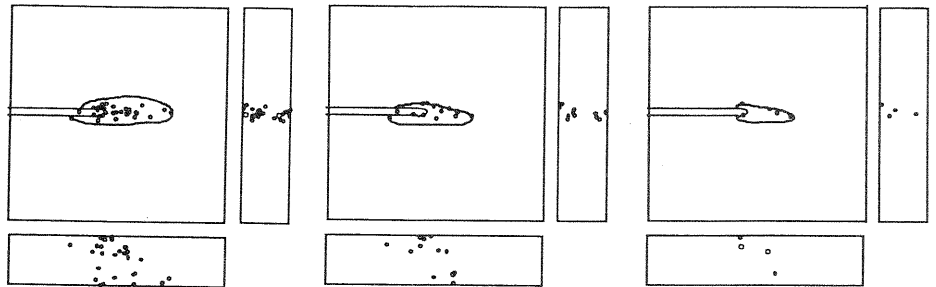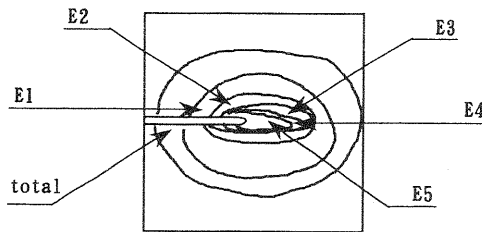
11

Fig.11. Distribution of calculated AE energy

(a)All events, (b) Higher than 100 $volt^2 \mu s$, (c) Higher than 1,000 $volt^2 \mu s$

(d)Higher than 10,000 $volt^2 \mu s$, (e)Higher than15,000 $volt^2 \mu s$, (f)Higher than 20000 $volt^2 \mu s$

(g) Comparison of the six energy stages by s.

Fig. 12. Maps of the AE event source location screened by energy stages at peak load.

Figure 12 shows maps of the AE event source location screened by five energy stages at peak load for M-type specimens. The AE events used in this calculation were those registered during the period between zero and peak load. Figue 12(a) shows a map of all the events. Figure 12(b), 12(c), 12(d), 12(e), and 12(f) show maps of events higher energy than 100 $volt^2 \mu$ s, 1,000 $volt^2 \mu$ s, 10,000 $volt^2 \mu$ s, 15,000 $volt^2 \mu$ s and 20 ,000 $volt^2 \mu$ s, respectiv ely. Figure 12(g) shows a schematic map of the 5 stages of AE energy drawned by making a boundary of the event's zone. It is obvious that the map for the higher energy events demonstrates a trend of localiza tion to the tip of the notch. The map of Fig. 12(b) still has a random distribution. In this paper, events that have energies higher than 1,000 $volt^2 \mu$ s are considered to be events related directly to the fracture process zones. The percentage of total energy of events higher than 1000 $volt^2 \mu$ s was 95.2 % of the total energy of all events.

Figure 13 shows the zones of AE events that an energy higher than 1,000 $volt^2 \mu$ s registered during five periods of load stages for M-type specimens. Figure 13(a), 13(b), 13(c), 13(d) , and 13(e) show zones of events registered during the period between zero to 0.3 peak load, 0.3
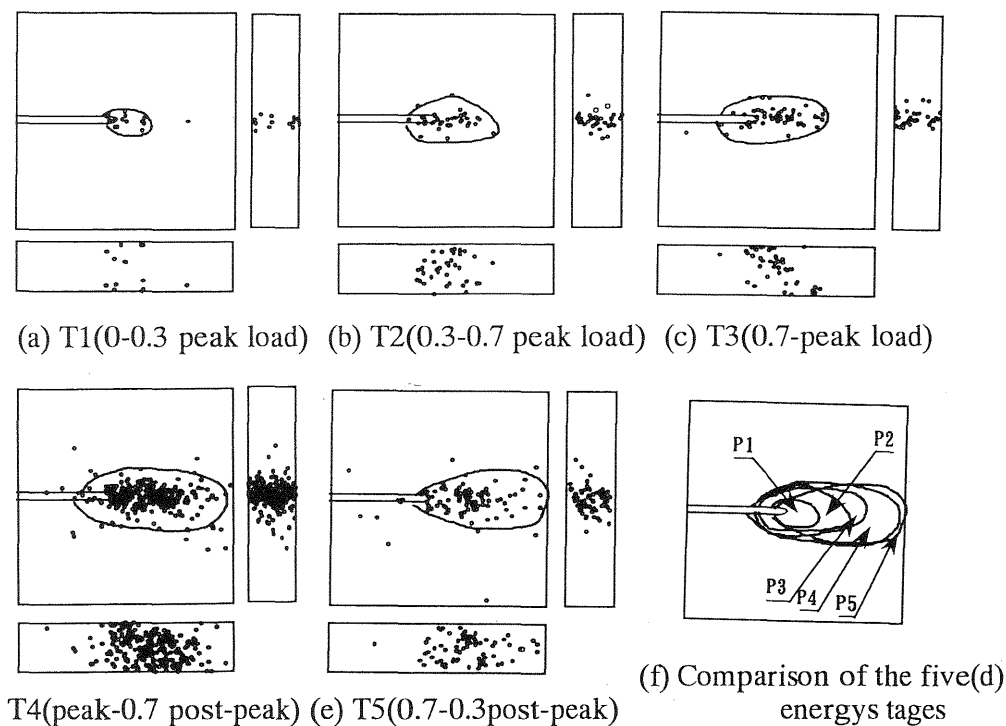

(a) T1(0-0.3 peak load) (b) T2(0.3-0.7 peak load) (c) T3(0.7-peak load)

T4(peak-0.7 post-peak) (e) T5(0.7-0.3post-peak)

(f) Comparison of the five(d) energys tages

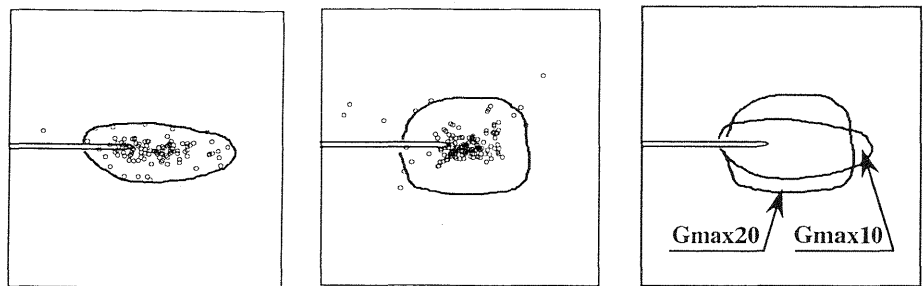Fig. 13. Progression of AE zone with loading

13

(Energy stage :1000 $volt^2\mu$ s)
peak load to 0.7 peak load, 0.7 peak load to peak load, peak load to 0.7
post-peak load, and 0.7 post-peak load to 0.3 post-peak load, respectively.

Fig. 13(f) shows a schematic map of AE events zones. At the first
load stage, a zone of AE events already occurred near the tip of the notch.
A trend can be observed from these figures that the zones of AE events
progress forward according to the load stages.

3.2.3 Influence of aggregate size on the fracture process zone

Figure 14 shows three zones of AE events higher than an energy of 1,000
$volt^2\mu$ s registered during a period from 0.3 pre-peak load to 0.3 post-peak
load for an M-type specimen. Figure 14(a) and14(b) show results obtained
for specimens made from concrete with maximum aggregate sizes of 10
mm and 20 mm, respectively. Figure14(c) is a schematic figure of the two
zones. A trend can be observed from these figures that the length of the
AE zone made by concrete with a maximum aggregate size of10 mm is
longer than that of 20 mm. A trend also can be observed that the width of
the AE zone made by concrete with a maxiumum aggregate size of 20 mm
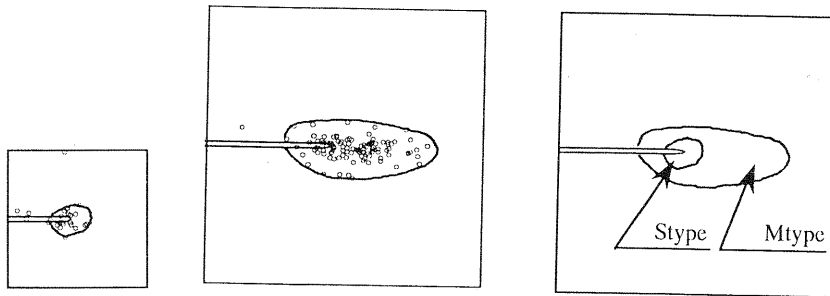is wider than that of 10 mm.

(a) Gmax : 10 mm   (b) Gmax : 20 mm   (c) Comparison
Fig. 14. Influence of maximum aggregate size on the AE zone

3.2.4 Influence of specimen size on AE zone

Figure 15 shows three zones of AE events higher than an energy of 1,000
$volt^2\mu$ s registered during the period between 0.3 pre-peak load and 0.3
post-peak load for S-type and M-type specimens. The maximum aggregate
size for both types of specimens was10 mm. Figure 15 (a) and 15(b) gives
the result obtained for the S-type and M-type specimens. Figure 15(c) is a
schematic figure of the two AE zones. From this figure, it can be seen that
the AE zone-length of M-type specimens is 4.3 times longer than that of
the S-type specimens. The ratio of AE zone-length is more than the ratio
of the specimen size. The AE zone width of the M-type specimen s is 2.0
times wider than that of the S type specimen. As the aggregate size of the

concrete for these two specimens was the same (10 mm), the width of their AE zones should not be significantly different. It therefore seems that the size of the S-type specimen was not enough to develop a fracture process zone.

(a) S type specimen   (b)   M type specimen   (c) Comparison
Fig. 15.   Influence of specimen size on the AE zone

3.3 Comparison of two methods

Figure 16 shows a comparison of the x-ray technique and AE technique methods. The lengths of the fine crack zones obtained by x-ray technique and the lengths of the energy zones of AE events obtained by AE technique are plotted in this figure. From this figure, it can be said that the AE method is more sensitive than the x-ray method in detecting the zone in which the fracture energy is used. The AE energy zones higher than 15,000 $volt^2 \mu$ s seem to be equal to the fine crack zones of the x-ray method.
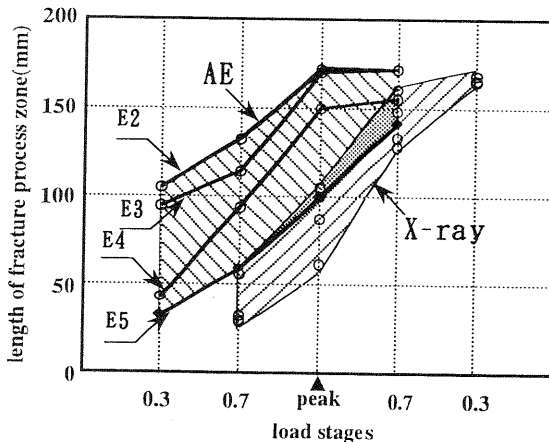

Fig . 16.   Comparison of two methods

4 Conclusion

Experiments were carried out by x-ray and AE techniques to investigate the behavior of the fracture process zone in concrete. From the results of these experiments, the following conclusions can be drawn.

1. Fine cracks in a complex configuration near the tip of the notch were observed by the x-ray technique with a contrast medium. The width of the crack zones increased with a larger maximum aggregate size, and the length of the crack zones decreased with larger maximum aggregate size. The length of the crack zones increased along with increases in the specimen size. The ratio of the increases in length is larger than the specimen size ratio.

2. The locations of AE event sources can be measured by three-dimensional AE technique. AE events occurred at the tip of the notch even at 0.3 peak load. The energy of each individual event could be calculated. Many events occurred which had a very small energy. A total of 45 % of these events made up only 0.5 % of the total energy of all events. The maps of higher energy events demonstrated a trend of localization to the tip of the notch. The zones of AE events progress forward according to the loading stages. The influences of aggregate and specimen size on the fracture process zone were measured. The trend of the influences as observed by AE was the same as that obtained by the x-ray technique.

3. The size of the fracture process zone obtained for the smaller -sized S-type specimen seemed to not be suitable. It is thought that a proper specimen size may exist in concrete for developing a correct fracture process zone.

5. References

Otsuka, K. (1989) X-ray technique with contrast medium to detect fine cracks in reinforced concrete, **Fracture Toughness and Fracture Energy** (eds H. Mihashi et al.), Balkema, 521-534.

Otsuka, K. (1992) Detection of fracture process zone in concrete by means of x-ray with contrast medium, **Fracture mechanics of concrete structures** (eds Z. P. Bazant), FraMCoS 1, Elsevier applied science, 485-490.

Otsuka, K. (1994) Size effect in fracture process zone of concrete, **Size Effect in Concrete Structures** (eds H. Mihashi et al.), E.& F.N. Spon, London, 47-56.